Nanocrystalline hard magnetic alloys

J. I. Betancourt R.
Instituto de Investigaciones en Materiales, U.N.A.M.
Apdo. Post. 70-360, México D.F. 04510, México.

The recent progress on the understanding of the physical properties of nanocrystalline hard magnetic alloys, based on Rare earth-Iron-Boron (REFeB) compositions, are reviewed. The discussion includes: fundamental properties, crystal structure, coercivity mechanism, micromagnetic studies and recent applications of these functional alloys. Prospective of future developments are also included.

Keywords: Nanocrystalline magnetic alloys; permanent magnets.

La presente revisión trata sobre las propiedades físicas y avances recientes en aleaciones magnéticas duras nanocristalinas, basadas en la composicin tierra-rara-hierro-boro (TRFeB). Se incluyen en la discusión los siguientes aspectos: propiedades físicas fundamentales, estructura cristalina, mecanismos de coercividad, estudios de micromagnetismo y aplicaciones recientes de estas aleaciones funcionales. Se menciona también hacia donde se enfoca la investigación actual en este tema.

Descriptores: Aleaciones magnéticas nanocristalinas; imanes permanentes.

PACS: 75.50.Ww; 75.50.Tt

1. Introduction

Hard magnetic alloys (also known as "permanent magnets") can be defined in general as those materials able to produce a coherent magnetic field without an electric current flowing through them. The main physical macroscopic properties to be characterised in these materials are: the remanent polarisation, J_r, which indicates the surrounding magnetic field strength; the coercivity, H_c, which is a measure of the material ability to resist demagnetisation; the maximum energy density $(BH)_{max}$, which reflects the magnetic energy stored in the material and the Curie temperature T_c, for which the ferromagnetic-paramagnetic transition establishes the maximum material operating temperature.

Permanent magnets are indispensable in modern technology and their influence is still growing. They can be found in many components of electromechanical and electronic devices. For example, an average home has more than fifty devices containing permanent magnets and a standard family car contains at least ten. Permanent magnets are used also as components in a wide range of industrial applications, in regulating and measuring controls and in medical equipment. They also play an important role in information technology (prominent examples are voice coil motors in hard discs drivers, floppy disc drivers and CD Rom's).

The 20th century has witnessed quite an extraordinary development in hard magnetic materials. This development has been strengthened in the last few decades, after the advent of rare-earth (RE) permanent magnets, in particular. This type of magnetic material is based on intermetallic compounds of a RE metal and cobalt or iron. They derive their exceptional properties from the favourable combination of properties of each RE sublattice and the 3d sublattice, the former mainly providing the magnetic anisotropy, the latter giving a high magnetisation and high ordering temperature.

Following the discovery and development of $SmCo_5$ and Sm_2Co_{17} magnets during the late 1960's and the 1970's important further advance in RE permanent magnet research was made in 1984, when a new ternary hard magnetic compound $(Nd_2Fe_{14}B)$ was announced by two independent groups; Croat *et al.* [1] at General Motors Co., USA and Sawaga *et al.* [2] at Sumitomo Metals, Japan. Using different techniques (melt spinning in the former case and powder metallurgy in the latter), they developed: a) thin ribbons consisting of ultrafine randomly oriented grains of the $Nd_2Fe_{14}B$ phase, with mean diameter typically less than 100 nm, and typical magnetic properties: $J_r = 0.8$ T, $H_c = 1120$ kA/m and $(BH)_{max} = 112$ kJ/m^3 and b) anisotropic magnets based on aligned and sintered 10 μm size particulate with typical magnetic properties: $J_r = 1.2$ T, $H_c = 1000$ kA/m and $(BH)_{max} = 288$ kJ/m^3.

Since their discovery, hard magnetic materials based on REFeB have been extensively studied [3-5]. Much of the work carried out thus far has been concentrated on NdFeB alloys but PrFeB magnets have received much attention lately [6]. In both cases, it has been shown that if the $RE_2Fe_{14}B$ grain size is refined to a nanophase structure (less than ~ 40 nm) [7-10] it is possible to enhance the remanence and the energy product as a result of exchange coupling between the resultant magnetic moment in each crystallite. This grain refinement can be achieved by controlling the processing conditions and influenced in some cases by addition of grain refining elements to the base REFeB. The advantage of substituting Nd for Pr in the $RE_2Fe_{14}B$ phase, particularly in cases such as nanocomposite alloys, where the coercivity is decreased substantially because of exchange coupling, is the higher coercivity shown by the $Pr_2Fe_{14}B$ phase [9] than for the Nd equivalent, due to its higher anisotropy field H_A [11]. Moreover, the Pr-based phase shows no spin reorientation at low temperature [12], unlike its Nd-based counterpart.

2. Crystal structure of REFeB unit cell

The exact stoichiometry and crystal structure of $Nd_2Fe_{14}B$ were first established by neutron powder diffraction analysis [13]. Figure 1 shows the $Nd_2Fe_{14}B$ unit cell, which corresponds to the space group $P4_2/mm$ tetragonal symmetry. The unit cell contains 68 atoms and consists of four formula units. There are six crystallographically different iron sites, two different rare-earth positions and one boron site. All the Nd and B atoms with four Fe(c) atoms of a total of 56, reside in the $z=0$ and $z=1/2$ mirror planes.
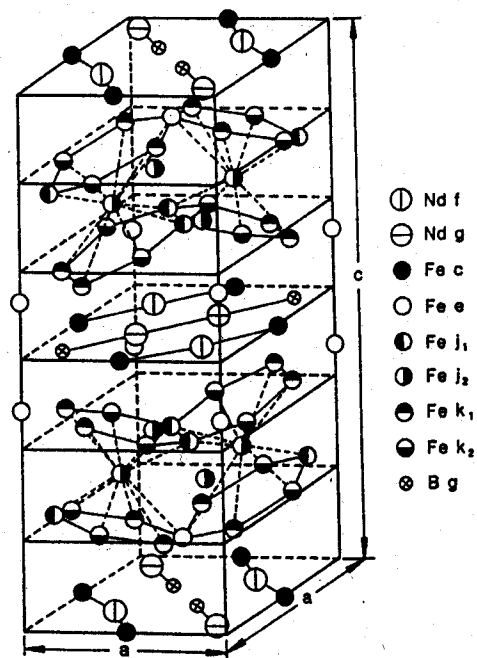

○ Nd f ⊖ Nd g
○ Fe e ● Fe k₁
⊗ B g

FIGURE 2.   Trigonal prism containing a boron atom in the $Nd_2Fe_{14}B$ structure.

⊕ Nd f
⊖ Nd g
● Fe c
○ Fe e
◑ Fe j₁
◐ Fe j₂
⊖ Fe k₁
⊖ Fe k₂
⊗ B g

FIGURE 1. Tetragonal unit cell of $Nd_2Fe_{14}B$.

The boron coordination in this compound shows interesting characteristics: each boron occupies the centre of a trigonal prism, Fig. 2, formed by the three nearest iron atoms above and the three below the basal plane. These prisms link Fe layers above and below the planes containing Nd and B and contribute in this way to the stability of the structure. Such prisms have been observed in other transition metal-metalloid systems (Fe_3B, Fe_3C, Fe_3P) and are fundamental for the formation of such phases [14].

The $RE_2Fe_{14}B$ structure forms for all the RE elements, except europium and promethium. As the atomic number Z increases in the $RE_2Fe_{14}B$ compound series, the c lattice parameter for the $RE_2Fe_{14}B$ phase decreases as a consequence of the progressive decrease in the radius of the trivalent RE ion, an effect which is known as "lanthanide contraction". On the other hand, the a lattice parameter decreases more slowly with Z, which suggests that the basal-plane dimension is influenced more by the stability of the Fe-B prisms than by the size of the RE ions.
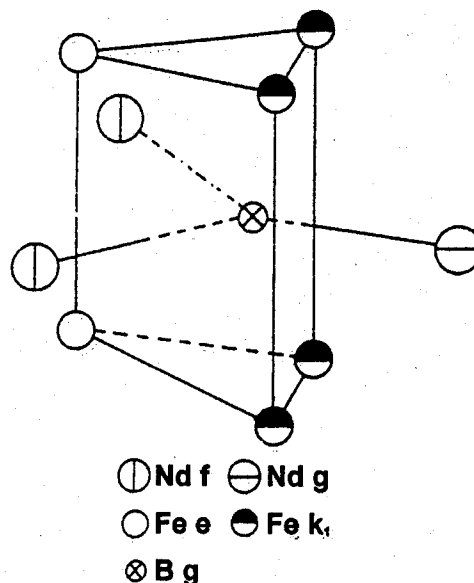
There are only two other known families of $RE_2TM_{14}B$-type compounds in which Fe or B is totally replaced by another element: $RE_2Co_{14}B$ and $RE_2Fe_{14}C$. Partial substitutions of RE, Fe or B, in which the $RE_2Fe_{14}B$ structure is preserved, are possible with many other elements, including the interstitial hydride series $RE_2Fe_{14}BH_x$ and $RE_2Co_{14}BH_x$.

3. Intrinsic magnetic properties of $RE_2Fe_{14}B$ compounds

Table I shows the intrinsic magnetic properties T_c (Curie temperature), J_s (saturation polarization), K_1, K_2 (anisotropy constants) and H_A (anisotropy field) at room temperature for the different $RE_2Fe_{14}B$ compounds. Those with RE corresponding to light rare-earths (La-Sm) have significantly higher values of saturation polarisation than those based on the heavy RE metals, due to the ferromagnetic RE-TM magnetic coupling in the former case, and to the antiferromagnetic RE-TM magnetic coupling in the latter [3]. The anisotropy fields H_A corresponding to these compounds are high, with maximum values at RE = Pr, Nd, Sm, Tb and Dy. This excellent H_A facilitates high coercivities values. An important drawback are the rather low Curie temperatures, which do not overcome 350°C. $Nd_2Fe_{14}B$ shows spin reorientation at 135 K at which the easy direction becomes canted at an increasing angle θ (between the easy direction and the c axis) with decreasing temperature, up to a maximum of $\theta = 30°$ close to 0 K [3]. $Pr_2Fe_{14}B$ on the other hand, shows no spin reorientation, being, for this reason, more suitable for low temperature applications than its Nd counterpart. This spin reorientation is a phenomenon reflecting a temperature dependent competition between the different RE site anisotropies in the $RE_2Fe_{14}B$ crystal structure [12].

TABLE I. Magnetic properties of $RE_2Fe_{14}B$ compounds at room temperature.

Compound	T_c(°C)	J_s(T)	K_1 (10^6J/m^3)	K_2 (10^6J/m^3)	H_A(T)
La$_2$Fe$_{14}$B	243	1.27			2.0
Ce$_2$Fe$_{14}$B	149	1.17	1.44		3.0
Pr$_2$Fe$_{14}$B	292	1.56	5.5		8.7
Nd$_2$Fe$_{14}$B	312	1.61	4.3	0.65	6.7
Sm$_2$Fe$_{14}$B	339	1.52	-12	0.29	15 (plane)
Gd$_2$Fe$_{14}$B	386	0.89	0.9		2.5
Tb$_2$Fe$_{14}$B	347	0.66	5.9		22
Dy$_2$Fe$_{14}$B	319	0.71	4.0		15
Ho$_2$Fe$_{14}$B	300	0.80	4.8		7.5
Er$_2$Fe$_{14}$B	278	0.89	-0.03		0.8 (plane)
Tm$_2$Fe$_{14}$B	267	0.92	-0.03		0.8 (plane)
Yb$_2$Fe$_{14}$B	250	1.20			
Lu$_2$Fe$_{14}$B	262	1.18			2.6
Y$_2$Fe$_{14}$B	298	1.41	1.1		2.0
Th$_2$Fe$_{14}$B	208	1.41			2.6

4. The origin of coercivity in REFeB permanent magnets

The origin of coercivity in rare-earth permanent magnets is the uniaxial magnetocrystalline anisotropy. Coercivity is not an intrinsic magnetic property, since it depends not only on the chemical compositions, the temperature and the magnetic anisotropy, but also strongly on the microstructure of the materials.

Nucleation models of coercivity are based on the assumption that, at large fields, all domain walls are removed. A single phase uniaxial magnet with anisotropy K ($K > M_s^2$) will thus behave as a large single domain particle. The magnetisation of this particle can be reversed at a field H_c, given by $H_c = H_k = (2K)/M_s$. This equation predicts H_c values ranging a factor 3-5 times larger than those realised in practice. This important discrepancy is known as Brown's paradox because, from a theoretical point of view, such reduction of H_N is not expected. To explain this discrepancy, it was assumed that nucleation takes place at secondary phases with lower K and/or at grains with large demagnetising factors N (grains with sharp corners) where the nucleation fields H_N are smaller, and given by [15]:

$$H_N = H_K - NM_s. \qquad (1)$$

According to the nucleation model, coercivity should increase with decreasing density of defects.

On the other hand, in domain wall pinning models, the inhomogeneities present in the magnet can prevent free domain wall motion, leading to higher H_c. Therefore, H_c should increase with increasing density of defects.

For *sintered magnets*, the prevailing view is that, at room temperature, they are nucleation-controlled systems [16],

with domain wall pinning playing a minor role. Domain observations show that, in the thermally demagnetised state, each Nd$_2$Fe$_{14}$B grain has a multidomain structure and that domain walls inside each grain move very easily in small applied fields. An analysis of the temperature dependence also suggest a nucleation controlling mechanism for sintered Nd-FeB magnets [17]. According to this, H_c can be written as

$$\mu_o H_c = \mu_o \alpha_K H_N^{min} - N_{eff} J_s, \qquad (2)$$

where N_{eff} is an average effective demagnetisation factor, describing the internal stray fields acting on the grains and $H_N^{min} = \alpha_\Psi H_N^{ideal}$ is the nucleation field for the most unfavourably aligned grains having a misalignment angle of 45° according to the Stoner- Wohlfarth [18] model. H_N^{ideal} is the theoretical nucleation field for perfectly oriented particles and is given by

$$H_N^{ideal} = \frac{2K_1}{J_s}$$

for vanishing higher order anisotropy constants. α_Ψ describes the reduction of the nucleation field due to the misorientation of the grains and α_K is related to the reduced surface anisotropy of nonperfect grains.

When the second order anisotropy constant K_2 is no longer negligible, H_N^{min} becomes [19]

$$H_N^{min} = \frac{1}{\sqrt{2}J_s\mu_o}\left[K_1 + \frac{K_2}{4}\left(W - K_1K_2 + 3\right)\right]$$
$$\times\sqrt{W\left(\frac{K_1}{K_2} + 1\right) - \left(\frac{K_1^2}{K_2} - \frac{2K_1}{K_2} + 3\right)}, \qquad (3)$$

where

$$W = \sqrt{\left(\frac{K_1}{K_2} + 1\right)^2 + 8} \quad \text{for } K_2 > 0 \text{ and } K_1 > -2K_2$$

or

$$W = -\sqrt{\left(\frac{K_1}{K_2} + 1\right)^2 + 8} \quad \text{for } K_2 < 0 \text{ and } K_1 > 0.$$

For small K_2 ($0 < K_2 < 0.5K_1$), an approximate expression for H_N^{min} can be derived from Eq. (3):

$$H_N^{min} \approx \frac{1}{J_s}\left(K_1 + K_2\left(1 + \frac{1}{2}\frac{K_2}{K_1} - \frac{1}{2}\left(\frac{K_2}{K_1}\right)^2\right)\right) \qquad (4)$$

For vanishing K_2 values, H_N^{min} is simply

$$H_N^{min} = \frac{1}{2}H_N^{ideal} = \frac{K_1}{J_s} \qquad (5)$$

As a consequence of the research on coercivity mechanisms, important suggestions for the improvement of sintered magnets are to achieve: a) small $RE_2Fe_{14}B$ grains in order to reduce the volume affected by reverse domain nucleation at a defect, b) grain boundaries as smooth as possible to limit the deleterious effects of local demagnetising fields at sharp edges, and c) a thin, smooth, defect-free grain boundary layer in order to magnetically isolate the $RE_2Fe_{14}B$ crystallites and provide a barrier to demagnetisation of neighbouring grains.

For *melt spun materials*, there is no an unanimous agreement about the origin of coercivity. Lorentz microscopy investigations show that domain walls tend to be pinned at grain boundaries in ribbons having optimum properties [20, 21].

Some authors [22, 23] reported good agreement between their measured values of coercivity with the domain wall pinning model of Gaunt [24], in which H_c is given by:

$$\left(\frac{H_c}{H_o}\right)^{1/2} = 1 - \left(\frac{75k_BT}{4bf}\right)^{2/3}, \qquad (6)$$

where H_o is the critical field in the absence of thermal activation, 4b is the range of the interaction between the domain wall and the pinning centre, f is the maximum restoring force per pinning centre and kB is the Boltzmann constant.

However, some other authors [16, 25-28] obtained good agreement between the measured H_c (as a function of temperature) data for melt spun alloys and those predicted by Eq. (2) with α_Ψ and α_K values ranging from 0.58 to 1 and 0.42 to 0.87, respectively, They thus concluded that melt-spun ribbons are nucleation-controlled systems for $T \leq 520$ K.

5. Effect of grain size on the magnetic properties

Stoner and Wohlfarth [18] developed a theory for a material based on non-interacting uniaxial magnetic particles which are uniformly magnetised along their easy axis of magnetisation. They predicted that J_r should have half the value of J_s for a material with randomly oriented crystallites, *i.e.*, $J_r/J_s = 0.5$. For conventional microcrystalline melt spun NdFeB alloys (mean grain size d_g of 60-100 nm) having a stoichiometric or near stoichiometric composition, J_r is found to be $0.5J_s$ [1, 7] which means that they obey the Stoner-Wohlfarth model. These materials were single phase $Nd_2Fe_{14}B$.

However, it is possible to enhance the remanence above the limit of $0.5J_s$ imposed by the Stoner-Wohlfarth model by means of the exchange coupling interaction. This exchange interaction in a polycrystalline REFeB aggregate is always present provided that grains are not decoupled by intergranular RE-rich phase but, it is not significant for $d_g \geq 40\text{-}50$ nm, since the total exchange volume is a very small fraction of the total grain volume. The exchange coupling effect is exerted at a characteristic length scale called exchange length, which is of the same order of magnitude as the domain wall width of the hard $Nd_2Fe_{14}B$ phase ($\sim$4 nm). Thereby, this exchange coupling is considered to occur in the outer 4 nm of each

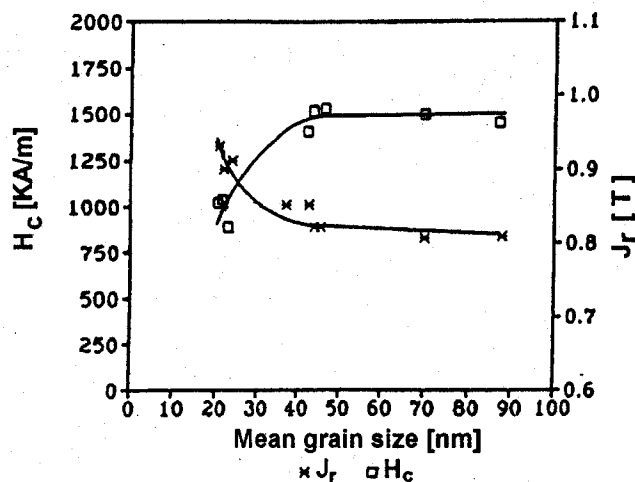FIGURE 3. Dependence of remanence J_r and coercivity H_c on grain size for melt spun $Fe_{70.6}Nd_{13.2}B_6Si_{1.2}$ [8]

2/14/1 grain and becomes progressively more significant as d_g is decreased into the nanocrystalline range. This results in a increasingly enhanced remanence and energy product. This effect was clearly demonstrated in ref [8]: as the mean grain size is refined below 40nm, the remanence is progressively enhanced and the coercivity is correspondingly reduced, Fig. 3.

6. Exchange spring magnets

A second class of remanence enhanced nanostructures are the *exchange spring* systems (or nanocomposites), so described in 1991 by Kneller and Hawig [29]. They investigated the combined effect of two suitably dispersed and mutually exchange-coupled phases (or exchange coupled composite material). The first of these phases (h) is a magnetically hard material, with large anisotropy constant K_h, providing high coercivity. The second one (s) is magnetically soft, with a higher magnetic ordering temperature, and therefore, higher exchange constant A_s. This s phase also lead to better remanence values due to its higher saturation polarization.

The critical dimension for the s phase b_s (= its domain wall width δ_s) depends on the magnetic coupling strength of the soft phase A_s and the magnetic anisotropy of the hard phase K_h, according to the relation

$$b_s = \pi \left(\frac{A_s}{2K_h}\right)^{1/2}. \qquad (7)$$

Using representative values of $A_s \sim 10^{-11}$ J/m, and $K_h \sim 10^6$ J/m^3 results in a value of $b_s \sim 5$ nm, which is about the same magnitude as b_h, *i.e.* $b_s \approx b_h$. It was proposed that the ideal microstructure should be the result of homogeneous precipitation of a h-phase in an s-phase, and not vice versa, giving a crystallographically coherent structure.

The first experimental observation of the exchange spring effect was by Coehoorn et al. [30], in melt spun Nd poor $Nd_4Fe_{78}B_{18}$ alloys, in which the hard phase $Nd_2Fe_{14}B$ contained only $\sim$ 15 % of the Fe atoms and the soft phases, mainly Fe_3B with a small amount of α- Fe, were predominant. Similarly, increased remanence enhancement was reported in the melt spun sub-stoichiometric $Nd_9Fe_{85}B_6$ alloys [31]. In these, the major phase was $Nd_2Fe_{14}B$ with α-Fe being the minority soft phase. This has the advantage over the $Nd_4Fe_{78}B_{18}$ alloy in that α-Fe has a larger J_s than Fe_3B and that H_c is larger because of the larger volume fraction of hard phase in the alloy. Further microstructural investigations on this system [32] confirmed that the nanoscale structure consisted of $Nd_2Fe_{14}B$ as the main phase, with mean grain diameter of $\sim$30 nm, and smaller α-Fe ($\sim$15 nm) crystallites of a second phase located as isolated particles interspersed throughout the microstructure.

7. Micromagnetic simulations

During the last few years, computer simulations of the magnetisation reversal behaviour based on finite element calculations of realistic microstructures, have become an important tool for studying microstructural effects in both stoichiometric single phase nanostructures and nanocomposite magnets [33-38].

The theoretical background for studying magnetisation processes in ferromagnetic materials is the continuum theory of micromagnetism. The aim of micromagnetic calculations is to derive the basic magnetic properties from the intrinsic material parameters and from the microstructure.

The method consist of minimisation of the total magnetic Gibbs free energy in an applied field, with respect to the magnetic polarisation J_s, subject to the constraint that $|J_s|$ is constant, which leads to a stable equilibrium state of a magnetic structure. The magnetic Gibbs free energy Φ_t of a ferromagnetic specimen in an applied magnetic field is the sum of several energy terms:

$$\Phi_t = \Phi_H + \Phi_S + \Phi_{ex} + \Phi_K \qquad (8)$$

The energy terms can be characterised by their effects on the magnetic polarisation J_s. The magnetostatic energy, Φ_H, tries to rotate J_s parallel to the external field. The stray field energy, Φ_S, favours the existence of magnetic domains. The exchange energy, Φ_{ex}, aligns the magnetic moments parallel to each other. The magnetocrystalline anisotropy energy, Φ_K, causes J_s to be preferably oriented along certain easy crystalline directions.

Calculations for both, single phase stoichiometric nanocrystalline $Nd_2Fe_{14}B$ magnets and nanocomposite α-$Fe/Nd_2Fe_{14}B$ have been reported [33]. Both studies have confirmed that the magnetic properties of isotropic nanostructured magnets are extremely sensitive to the microstructural features such as grain size, particle shape, intergranular layers and the volume fraction of the soft magnetic phase.

For single phase magnets in a regular grain arrangement (i.e. directly contacted grains), it has been confirmed [33] that for d_g below $\sim$40 nm, enhancement of the remanence above $0.5J_s$ becomes progressively larger (with decreasing d_g), while the coercivity decreases, fact that is consistent with earlier experimental observations [8]. In the same study, results for nanocomposite magnets are also included. Further remanence enhancement is achieved with increasing soft phase volume fraction, with the consequent deleterious effect on the coercivity, again consistent with experimental observation [39]. However, the maximum energy product shows higher values with increasing soft phase volume fraction. This numerical investigation suggests an optimal microstructure consisting of small soft magnetic grains (main grain diameter $\sim$10 nm, volume fraction of $\sim$ 40%) embedded between hard magnetic grains with a mean grain diameter of about 20 nm. Additionally, a microstructure with regular shaped grains improves the magnetic properties.

8. Applications

Most of the nanocrystalline REFeB-based magnets production goes to the computer industry (mainly hard disk drives) and for novel actuators and motors, in which a reduction in both weight and number of parts is desirable in order to achieve energy savings and improved reliability. Among the remaining applications are: magnetic resonance imaging, acoustics, high efficiency rare-earth magnet electric machines, novel digital signal processors, new power electronic components as shown in Fig. 4 [40,41]. All these applications benefits industrial, automotive, consumer white goods and office equipment industries.
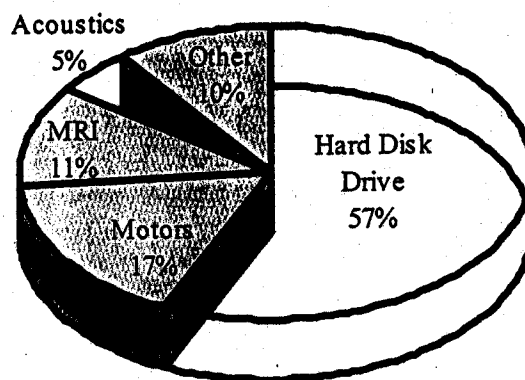

FIGURE 4. Applications for Nd-Fe-B magnets.

The specific application of nanocrystalline REFeB-based magnets in hard disk drives is the linear electromagnetic actuator which positions the read/write head [40]. This is commonly called a "voice coil motor" (or VCM). As the storage capacity of disk drives has risen, so too has the demand for faster data access times, and to achieve this the VCM needs to operate at the highest possible level of magnetic flux density.

Magnetic resonance imaging (MRI) is a more recent and rapidly growing market for fully dense Nd-Fe-B magnets. The importance of this market is driven by the fact that a single MRI scanner that is designed to accomodate and scan a whole human body, typically require about 1000 kg of Nd-Fe-B magnets. This in order to achieve the suitable magnetic fields for the scanning process [40].

Rare-earth magnets are also useful for levitation systems: a magnetic levitation system with $YBa_2Cu_3O_7$ superconductors and Nd-Fe-B magnets has been recently reported [42]. A stable levitation of the superconductor above magnets is possible without any regulation and feedback circuit. The system consists of an engine with two YBCO disks, 25 mm diameter, which are cooled with liquid nitrogen and a magnetic rail made of Nd-Fe-B magnets. The engine levitates 5 mm above the magnetic rail.

An emerging market is the electric vehicle industry, especially the hybrid electric car. A typical hybrid car contains 1-2 kg of Nd-Fe-B magnets [41], e.g. the air conditioning system and the navigation system on the car, among others, requires high efficient dc RE magnet motors.

9. Concluding remarks

Nanocrystalline REFeB-based magnets have attracted much attention since their discovery in 1984. Their outstanding combination of magnetic properties (very high H_c and J_r together with excellent $(BH)_{max}$ density values) enables them for an ample range of applications. Current research efforts are focused on novel compositions and processing techniques, addressed to achieve further enhancement of magnetic properties, since the theoretically predicted maximum energy density (around 1000 kJ/m^3) has not been attained yet. Micromagnetic simulations have played a central role in understanding the correlation between physical intrinsic properties and macroscopic parameters which, in addition, states new approaches for both, fabrication technology and applications.

1. J.J. Croat, J.F. Herbst, R.W.Lee and F.E. Pinkerton, *J. Appl. Phys.* **55** (1984) 2078.

2. M. Sawaga, S. Fujimura, N. Togawa and H. Yamamoto, *J. Appl. Phys.* **55** (1984) 2083.

3. J.F. Herbst, *Rev. Mod. Phys.* **63** (1991) 819.

4. J.M.D. Coey, *J. Mag. Mag. Mater.* **140-144** (1995) 1041.

5. K.H.J. Buschow, *Handbook of Magnetic Materials*, Vol.10. Ed. K.H.J. Buschow (Elsevier Science, Holland, 1997).

6. H.A. Davies, C. Harland, J.I.Betancourt, R G. Mendoza, *Proc. MRS Symp. on Advanced Hard and Soft Magnetic Materials*, Eds. Michael Coey *et al.* (Warrendale, USA, 1999) p. 27.

7. H.A. Davies, *J. Magn. Magn. Mat.* **157-158** (1996) 11.

8. A Manaf, R.A. Buckley and H.A. Davies, *J. Mag. Mag. Mat.* **101** (1991) 360.

9. I. Betancourt and H. A, Davies, *J. Appl. Phys.* **85** (1999) 5911.

10. D. Goll, M. Seeger and H. Kronmuller, *J. Magn. Mag. Mat.* **185** (1998) 49.

11. S. Hirosawa, Y Matsuura, H. Yamamoto and S. Fujimura, *J. Appl. Phys.* **59** (1986) 873.

12. C. Abache and H. Oesterreicher, *J. Appl. Phys.* **57** (1985) 4112.

13. J.F. Herbst, J.J. Croat and W.B. Yelon, *Phys. Rev. B* **29** (1984) 4176.

14. P.H. Gaskell, *Nature* **289** (1981) 474.

15. C. Burkhardt, M. Steinhorst and I.R. Harris, *13th Int. Workshop on RE Magnets and their Applications*, Eds. C.A.F. Manwaring *et al.* (University of Birmingham UK, 1994) p. 473.

16. K.D. Durst and H. Kronmuller, *J. Mag. Mag. Mater.* **68** (1987) 63.

17. H. Kronmüller, K.D. Durst and M. Sawaga, *J. Mag. Mag. Mater.* **74** (1988) 291.

18. E.C. Stoner and E.P. Wohlfarth, *Phil. Trans. Roy. Soc.* **240** (1948) 599.

19. G. Martinek, H. Kronmuller, *J. Mag. Mag.Mater.* **86** (1990) 177.

20. R.K. Mishra, *J. Mag. Mag. Mater.* **54-57** (1986) 450.

21. G.C. Hadjipanayis and R.C. Dickenson, *J. Mag. Mag. Mater.* **54** (1986) 557.

22. G.C. Hadjipanayis, K.R. Lawless and R.C. Dickenson, *J. Appl. Phys.* **57** (1985) 4097.

23. G. Hadjipanayis and A. Kim, *J. Appl. Phys.* **63** (1988) 3310.

24. P.Gaunt, *Phil. Mag. B* **48** (1983) 261.

25. M. Seeger, D. Kohler and H. Kronmuller, *J. Mag. Mag. Mater.* **130** (1994) 165.

26. J. Bauer, M. Seeger and H. Kronmuller, *J. Mag. Mag. Mater.* **139** (1995) 323.

27. De Julian, F. Cebollada and J.M. Gonzalez, *J. Appl. Phys.* **81** (1997) 4431.

28. I. Betancourt and H.A. Davies. (Accepted for publication in *Physica B*).

29. E.F. Kneller and R. Hawig, *IEEE Trans Magn.* **27** (1991) 3588.

30. R. Coehoorn and D.B. de Mooij, C. de Waard, *J. Mag. Mag. Mater.* **80** (1989) 101.

31. A. Manaf, R.A. Buckley and H.A. Davies, *J. Mag. Mag. Mater.* **128** (1993) 302.

32. A. Manaf, M. Al-Khafaji and H.A. Davies, *J. Mag. Mag. Mater.* **128** (1993) 307.

33. R. Fischer, J. Scherfl, H. Kronmuller and J. Fidler, *J. Mag. Mag. Mater.* **153** (1996) 35.

34. M.K. Griffiths, J.E.L. Bishop and H.A. Davies, *J. Mag. Mag. Mater.* **183** (1998) 49.

35. M.K. Griffiths, J.E.L. Bishop and H.A. Davies, *J. Mag. Mag. Mater.* **234** (2001) 331.

36. R. Fischer and H. Kronmuller, *Phys. Rev. B* **54** (1996) 7284.

37. H. Fukunaga and Y. Kanai, *Proc. 10th Int. Symp. on Magnetic Anisotropy and Coercivity in RE Transition Metal Alloys*, Eds. L.Schultz and K.H. Muller. (MATINFO, Frankfurt, 1998) p. 237.

38. H. Fukunaga and H. Inoue, *Jpn. J. Appl. Phys.* **31** (1992) 1347.

39. A.Manaf, M.Loeonowicz, H.A. Davies, and R.A. Buckley, *Mater. Lett.* **13** (1992) 194.

40. P. Campbell, *Proc. 15th Int. Workshop on RE Magnets & Aplications*, Eds. L.Shultz & K.H. Muller, (MATINFO, Frankfurt, 1998) p. 681.

41. R.E. Hanitsch, *Proc. 16th Int. Workshop on RE Magnets & Aplications*, Eds. H. Kaneko, M. Homma and M. Okada, (The Japan Institute of Metals, Sendai, 2000) p. 923.

42. P. Verges, *Proc. 15th Int. Workshop on RE Magnets & Aplications*, Eds. L.Shultz & K.H. Muller, (MATINFO, Frankfurt, 1998) p. 767.